A novel motif in calcimembrin/C16orf74 dictates multimeric dephosphorylation by calcineurin

Devin A. Bradburn[1,7], Joana C. Reis[2,3,7], Shariq Qayyum[2,4,5], Thibault Viennet[2,3,6], Haribabu Arthanari[2,3], Martha S. Cyert[1]*

1. Department of Biology, Stanford University, Stanford, CA 94305, USA
2. Department of Cancer Biology, Dana-Farber Cancer Institute, Boston, Massachusetts, USA.
3. Department of Biological Chemistry and Molecular Pharmacology, Harvard Medical School, Boston, Massachusetts, USA.
4. Men's Health: Aging & Metabolism, Brigham and Women's Hospital, Harvard Medical School, Boston, MA, USA.
5. Cardiovascular Research Center, Department of Medicine, Massachusetts General Hospital and Harvard Medical School, Boston, MA, USA
6. Department of Chemistry and iNANO, Aarhus University, Aarhus, Denmark
7. Contributed equally to this work

*Corresponding author:
Department of Biology
410B Bass Biology Building
Stanford University
Stanford, CA 94305-5020
phone: 650 723-9970
fax: 650 724-9945
E-mail: mcyert@stanford.edu

Significance Statement:

Many substrates and regulators of calcineurin, the conserved Ca^{2+}/calmodulin-regulated protein phosphatase and target of immunosuppressant drugs, are yet to be identified. We show that the intrinsically disordered and cancer-associated protein, calcimembrin, is a calcineurin substrate, contains a composite calcineurin-binding motif and is reversibly lipidated (S-acylated) to recruit calcineurin to membranes. *In vivo* and *in vitro* analyses, including nuclear magnetic resonance (NMR), show how the novel motif in calcimembrin binds calcineurin with extraordinarily high affinity and confers dephosphorylation in multimeric complexes containing two calcimembrin molecules bound to different sites on calcineurin. We propose that this unusual dephosphorylation mechanism confers unique properties to calcimembrin-associated calcineurin signaling. This work extends our understanding of how calcineurin and proteins containing such composite calcineurin-binding motifs function.

Abstract:

Calcineurin (CN), the only Ca^{2+}/calmodulin-activated protein phosphatase and target of immunosuppressant drugs, dephosphorylates substrates within membrane-associated Ca^{2+} microdomains. CN binds to substrates and regulators via short linear motifs (SLIMs), PxIxIT and LxVP, which have distinct docking sites on CN. PxIxIT binding to CN is Ca^{2+}-independent and affects its distribution, while LxVP associates only with the active enzyme and promotes catalysis. 31 human proteins contain one or more composite 'LxVPxIxIT' motifs, whose functional properties have not been examined. Here we study calcimembrin/C16orf74 (CLMB), a largely uncharacterized intrinsically disordered protein that contains a composite motif which binds to and directs CN to membranes. CLMB overexpression is associated with poor prognoses for several cancers, suggesting that it promotes oncogenesis by shaping CN signaling. We demonstrate that CLMB associates with membranes via N-myristoylation and dynamic S-acylation and is dephosphorylated by CN on threonine 44 (Thr44). The LxVP and PxIxIT portions of the CLMB composite sequence, together with Thr44 phosphorylation, confer high affinity PxIxIT-mediated binding to CN (K_D~8.3 nM) via an extended ^{33}LxVPxIxITxx(p)T^{44} sequence. This binding promotes CLMB-based targeting of CN to membranes, but also protects Thr44 from dephosphorylation. Thus, we propose that CLMB promotes dephosphorylation in multimeric complexes, where one CLMB molecule recruits CN to membranes via PxIxIT binding, allowing other proteins (including CLMB) to engage through their LxVP motifs for dephosphorylation. This unique mechanism makes dephosphorylation sensitive to CLMB:CN ratios and is supported by *in vivo* and *in vitro* data including nuclear magnetic resonance (NMR) analyses of CLMB alone and complexed with CN.

Introduction

Calcium (Ca^{2+}) ions are spatially and temporally controlled in cells to regulate a wide array of biological processes. Ca^{2+} signaling frequently occurs within membrane-associated microdomains that contain both effector proteins and their substrates. Thus, subcellular localization of calcineurin (CN), the only Ca^{2+}-calmodulin (CaM) regulated serine/threonine protein phosphatase, dictates its signaling specificity(*1*). CN interacts with partners via two short linear motifs (SLiMs), referred to as LxVP and PxIxIT, that cooperate to promote dephosphorylation. PxIxIT binding occurs independent of Ca^{2+}-signals and anchors CN to substrates, which increases local substrate concentration, and to regulators, such as scaffold protein A kinase anchoring protein 5 (AKAP5)(*2*), which directs CN to localized signaling domains. LxVP binding helps to orient substrates for dephosphorylation at a separate catalytic site, marked by a Zn^{2+} and Fe^{2+} ion(*3*). The LxVP docking site on CN is accessible only after activation by Ca^{2+}/CaM and is blocked by the autoinhibitory C-terminal tail of CN as well as the immunosuppressant drugs, Cyclosporin A and FK506(*4, 5*). Systematic identification of these SLiMs has significantly expanded our knowledge of CN substrates and functions(*6-9*) and identified 31 human proteins that contain a novel composite CN-binding motif where LxVP and PxIxIT occur in a single sequence with a shared proline (LxVPxIxIT)(*9*). Both SLiMs in a composite motif can bind their cognate sites on CN, but are unlikely to simultaneously engage these docking surfaces, which are ~60 Å apart. Thus, how or if these motifs promote dephosphorylation is unclear. Here we examine the function of a composite motif in C16orf74, a short, unstructured, and largely uncharacterized protein that is associated with poor outcomes in melanoma, pancreatic and head and neck cancer(*10, 11*). Because C16orf74 binds to and recruits CN to membranes(*10*), we have named it calcimembrin (CLMB).

In this work we show that CLMB associates with membranes via two lipid modifications, N-myristoylation and S-acylation, where it recruits CN. S-acylation, the only reversible protein lipidation, regulates many aspects of signaling at membranes(*12*). In addition to CLMB, S-acylation modulates CN activity through at least two additional mechanisms: S-acylation regulates subcellular localization of the AKAP5 scaffold in neurons to direct local CN signaling and control long-term synaptic potentiation(*13*). Also, the naturally occurring CN isoform, CNAb1, contains an S-acylated C-terminus, which promotes dephosphorylation of membrane-associated substrates such as the phosphatidyl-inositol-4-kinase IIIa (PI4KIIIIa) complex(*14*).

Previous studies showed that CLMB binding to CN required phosphorylation of Thr44 and was disrupted when the central 'PxIxIT' sequence was deleted, which also compromised the 'LxVP' portion of the motif(*10, 15*). Our studies carefully dissect the composite motif to elucidate how the PxIxIT and LxVP portions of this sequence make distinct contributions to CN-CLMB interactions. We demonstrate that CN

dephosphorylates CLMB at Thr44, which requires the 'LxVP' sequence. In addition, detailed binding and structural analyses show that the composite motif confers extremely strong PxIxIT-mediated binding to CN, which is strengthened by flanking LxVP and phospho-Thr44 features.

Furthermore, our work establishes that the composite LxVPxIxITxx(p)T motif confers unique signaling properties to CLMB. Using in-cell assays, together with *in vitro* dephosphorylation and kinetic modeling, we show that CLMB dephosphorylation is strongly influenced by the CLMB:CN ratio, supporting a model in which CN dephosphorylates CLMB in a multimeric 2:1 (CLMB:CN) complex, whose formation is also indicated by NMR analyses. We propose that one CLMB molecule provides a high affinity PxIxIT motif and recruits CN to membranes, where it dephosphorylates other proteins (including CLMB) via LxVP-mediated interactions. In summary, this work establishes that composite motifs not only mediate dephosphorylation but can also dynamically shape CN signaling.

Results

Calcimembrin is myristoylated and S-acylated. CLMB is a small, disordered protein with no predicted transmembrane domains (Figure 1A) that associates with membranes(*10*). We investigated whether protein lipidation might be responsible for this localization. CLMB contains an N-terminal glycine (G2), a common site for N-myristoylation, the co-translational addition of a 14-carbon lipid which often contributes to membrane association in combination with other lipid modifications(*16*). These include S-acylation, the reversible addition of a fatty acid, often a 16-carbon palmitate, to the sidechain of cysteine residues(*12*). CLMB has two cysteines near in its N-terminus, Cys7 and Cys14, one of which, Cys7, is predicted to be S-acylated(*17*). These cysteines have previously been implicated in CLMB dimer formation via disulfide bonds(*18*). To determine if CLMB is lipidated, we metabolically labeled HEK293 Flp-In T-REx cells inducibly expressing wildtype CLMB-FLAG ($CLMB_{WT}$) with YnMyr and 17-ODYA, alkyne-containing analogs of myristate and palmitate respectively(*19*). Following immunoprecipitation, analog incorporation was detected via addition of biotin using CLICK-chemistry followed by visualization with streptavidin (Figure 1B). $CLMB_{WT}$ incorporated YnMyr and 17-ODYA, indicating the presence of both lipids. To determine sites of lipidation, we mutated both C7 and C14 to serine ($CLMB_{C7,14S}$), which eliminated 17-ODYA incorporation while maintaining YnMyr incorporation. By contrast, neither lipid modification was detected for $CLMB_{G2A}$ (Figure 1B). We noted low expression of these mutants, suggesting that lipidation enhances protein stability. For this reason, a proteasome inhibitor (MG132) was included in all assays examining CLMB lipidation mutants.

To determine if CLMB-FLAG is dually S-acylated at Cys7 and Cys14, we used an acyl-PEG exchange assay in which S-acylated groups are cleaved using hydroxylamine (NH_2OH) and exchanged for a PEGylated molecule that increases protein mass by 5 kDa for each S-acylated residue(*20*) (Figure 1C). $CLMB_{WT}$ displayed two slower migrating bands representing singly- and dually S-acylated forms of the protein. $CLMB_{C7S}$ lacked the upper band, while $CLMB_{C7,14S}$ was unmodified, indicating that C7 and C14 of FLAG-$CLMB_{WT}$ are both S-acylated. $CLMB_{G2A}$ also displayed two sites of S-acylation in these analyses, suggesting that the metabolic labeling experiment (Figure 1B) was not sufficiently sensitive, given low protein expression, to detect these modifications. Together these findings suggest that CLMB is myristoylated at Gly2 and S-acylated at Cys7 and Cys14.

S-acylation of CLMB is dynamic and mediates membrane association. To examine the dynamics of CLMB-FLAG S-acylation, which turns over rapidly in some but not all proteins(*12*), we carried out a pair of pulse-chase analyses with two metabolic labels (Figure 1D and 1E). L-AHA, an azide-containing methionine analog detected CLMB-FLAG protein levels, while in parallel, 17-ODYA detected S-acylation. After a one-hour pulse, analogs were removed for a 30-minute chase with DMSO or Palmostatin B (PalmB), a small molecule pan-inhibitor of enzymes that reverse S-acylation(*21*), followed by immunopurification (IP) of CLMB-FLAG. Quantifying the 17-ODYA to L-AHA ratio showed that CLMB palmitate incorporation increased ~3-fold when de-S-acylation was inhibited (PalmB vs DMSO). Thus, CLMB S-acylation, which turns over rapidly relative to protein degradation, is dynamic.

To determine if lipidation mediates CLMB membrane recruitment, we utilized detergent assisted subcellular fractionation. While $CLMB_{WT}$ was primarily found in membrane fractions, both $CLMB_{G2A}$ and $CLMB_{C7,14S}$ were predominantly cytosolic (Figure 1F and 1G). Therefore, N-myristoylation and dynamic dual S-acylation of CLMB stabilize the protein and mediate its associate with membranes.

The composite SLiM in CLMB mediates binding to and dephosphorylation by calcineurin. Because CLMB contains an unusual composite LxVPxIxIT motif, LDVPDIIIT, we examined how each part of this sequence might function with respect to CN by generating two mutants, $CLMB_{IxITMut}$ (LDVPD**AIAA**) and $CLMB_{LxVMut}$, (**AD**A**P**DIIIT) (Figure 1A) to disrupt each motif separately without altering the shared proline. To examine binding of these mutants to CN, CLMB-FLAG constructs and GFP-tagged CN (CNA-GFP) were co-transfected into HEK293 cells, with immunoprecipitation of CNA-GFP from these lysates used to assess association with CLMB (Figure 2A and 2B). $CLMB_{WT}$ co-immunoprecipitated with CNA-GFP and this interaction was PxIxIT dependent, as $CLMB_{IxITMut}$ failed to co-purify. This is consistent with demonstrated roles for PxIxIT motifs mediating stable association with CN(*5*). $CLMB_{LxVMut}$ displayed reduced co-purification, indicating that, to a lesser extent, it also contributes to CN binding. Furthermore,

the input samples showed that both mutants displayed a second slower mobility band which is also faintly observed for $CLMB_{WT}$, albeit with a decreased electrophoretic mobility shift. These slower migrating forms represent CLMB that is phosphorylated at Thr44 and are eliminated when this residue is mutated to alanine ($CLMB_{T44A}$, $CLMB_{T44A+LxVMut}$). This observation suggests that CLMB binds to and is dephosphorylated by CN, and that disrupting either the LxVP or PxIxIT portion of the composite motif prevents dephosphorylation. Finally, we observed that the slower migrating form of both $CLMB_{WT}$ and $CLMB_{LxVMut}$ predominantly co-purified with CN, suggesting, as previously reported, that phosphorylation at Thr44 enhances binding to CN(*10*). Indeed, $CLMB_{T44A}$ displayed reduced binding to CN, which was further reduced by also mutating LxV ($CLMB_{T44A+LxVMut}$).

The contributions of the PxIxIT, LxVP, and Thr44 phosphorylation to binding are also reflected in the ability of CLMB to recruit CN to membranes. Immunofluorescence (IF) shows that $CLMB_{WT}$-FLAG recruits CN-GFP to membranes, when co-transfected into MCF7 cells (Figure 2C, 2D). However, CN is largely cytosolic and colocalizes poorly when co-expressed with $CLMB_{IxITMut}$. $CLMB_{LxVMut}$ and $CLMB_{T44A}$ show minor but significant reductions in colocalization with CN, mirroring the trends observed with co-immunoprecipitation experiments.

Dephosphorylation of Thr44 by CN was confirmed *in vitro* using a phosphorylated peptide substrate encoding residues 21-50 of CLMB (Figure 1A and 2 E). In contrast, a peptide encoding the sequence from $CLMB_{LxVMut}$ failed to be dephosphorylated showing that, like other CN substrates, the LxVP motif is required for dephosphorylation(*22*). Together, these data show that both the LxVP and PxIxIT components of the composite motif are functional, that CLMB is a CN substrate, and that Thr44 phosphorylation enhances CLMB binding to CN.

Phosphorylation and the LxVP motif enhance PxIxIT binding. To quantitatively assess components of CLMB binding to CN, we used isothermal titration calorimetry (ITC) and fluorescence polarization anisotropy (FP) to measure binding affinities between CLMB peptides containing the composite SLiM (residues 21-50) and the catalytically inactive $CN_{Trunc+H151Q}$, which lacks the C-terminal autoinhibitory region of CNA, allowing LxVP motifs to bind to CNA/B heterodimers independent of Ca^{2+}/CaM(*23*). ITC revealed that the phosphorylated $CLMB_{WT}$ peptide ($pCLMB_{WT}$) binds CN at a one-to-one ratio with the highest reported affinity for a CN substrate, (K_D= 8.29 nM), (Figure 3A). FP using FITC-labelled peptides revealed ~30-fold stronger binding for the phosphorylated vs non-phosphorylated peptide (K_D = 12.29nM vs 384.5 nM (Figure 3B). The concordance between ITC, which utilized a tag-free CLMB peptide, and FP, which employed a fluorescein-tagged peptide (8.29 vs 12.29 nM for $pCLMB_{WT}$), suggests that the tag does not significantly affect binding affinity. Given the high-throughput capability of FP, it was used for the

remaining comparisons. To test if the high affinity $pCLMB_{WT}$-CN binding observed was PxIxIT-mediated, we used FP to assess the ability of CLMB peptides to compete for CN binding with PVIVIT, a well characterized PxIxIT peptide(*24, 25*) (Figure 3C). $pCLMB_{WT}$ competed with PVIVIT most effectively, (Figure 3C, 3E) with decreased competition exhibited when the LxVP motif was mutated ($pCLMB_{LxVMut}$), or Thr44 was not phosphorylated ($CLMB_{WT}$). $pCLMB_{IxITMut}$ lacking the PxIxIT motif was unable to displace PVIVIT from CN. A very similar pattern was observed when these experiments were repeated using $pCLMB_{WT}$ peptide in place of PVIVIT (Figure 3D, 3E), suggesting that like PVIVIT, $pCLMB_{WT}$ also engages CN primarily through the PxIxIT motif. Altogether, these data show that CLMB binding to the PxIxIT docking groove on CN is enhanced by residues flanking the core PxIxIT, i.e. LxV and phospho-Thr44, to form an extended LxVPxIxITxxT(p) sequence with exceptionally high affinity for CN.

NMR analysis of CLMB with calcineurin suggests multimeric interactions. Next, to investigate the structure of CLMB in the presence and absence of CN, we used solution-state NMR. 88% of non-proline backbone resonances were assigned using a standard set of triple-resonance experiments, utilizing full-length dually ^{13}C- and ^{15}N-labeled CLMB (76 residues) that was expressed in *E.coli* where it is neither phosphorylated nor lipidated (Figure 4A and S1A). To assess CLMB secondary structure, we employed Talos-N, a computational method that predicts backbone torsion angles from NMR chemical shifts. This revealed that although CLMB is disordered overall, two regions, including the PxIxIT motif (residues I38-I40), displayed a tendency to form a β-strands, which is characteristic of binding at the PxIxIT docking groove on CN (Figure S1B)(*4, 26*). A similar pattern was observed for the N-terminus Q12-V15 which may be predisposed to localized folding and involved in other binding interactions.

To map the interaction interface of CN on CLMB, we focused first on PxIxIT-mediated interactions by titrating ^{15}N-labeled CLMB with varying molar ratios of monomeric calcineurin A (CNA) and monitoring the interaction through ^{15}N-^{1}H SOFAST-HMQC experiments. CNA can bind to PxIxIT motifs but lacks the LxVP binding surface found at the interface of CNA and CNB(*4*). Due to the size of the CLMB-CN complex, we anticipated significant broadening of NMR signals at the interaction interface. This broadening of NMR resonances can also arise from the exchange kinetics between the observable CLMB and the titrant, CNA, making it challenging to distinguish the two effects. As expected, at a molar ratio of 2:1 (CLMB: CNA), many of the CLMB signals undergo significant line broadening, which become more pronounced at a molar ratio to 1:1when the majority of CLMB is bound to CNA. This is particularly the case for signals corresponding to the PxIxIT and LxVP motifs, indicating, as observed in FP experiments, that LxV residues participate in binding to the PxIxIT interface (Figure 4B and C, Figure S1C). Line broadening across the majority of CLMB residues indicates that the interaction interface on CLMB extends beyond the PxIxIT and LxVP motifs (Figure 4B and C). Interactions with these N- and C-terminal residues of CLMB may be

an avidity-driven effect, anchored by PxIxIT binding, with similar phenomena reported for other CN substrates(*27*).

To investigate binding that may occur at the LxVP docking site of CN, we next titrated CLMB with the heterodimeric CNA/B complex. Signal broadening at the N-terminus of CLMB was more pronounced with CNA/B relative to CNA alone, suggesting possible interactions between CLMB and CNB (Figure 4B, C vs 4D, E, and S1D). At a molar ratio of 2:1 (CLMB: CNA/B), more broadening is observed in LxVP but not PxIxIT residues when compared to the interaction with CNA (Figure 4B vs 4D, and S1C). However, at a molar ratio of 1:1, where essentially all CLMB should be PxIxIT-bound (given the higher K_D and our working concentrations), the pattern of line broadening at the composite motif is similar with the addition of CNA or CNA/B (Figure 4C vs 4E). Together this indicates that when in excess (2 CLMB: 1 CN), CLMB engages CNA/B through both its LxVP and PxIxIT motifs. To investigate these interactions further, we carried out structural predictions for 2 phosphorylated CLMB molecules and CNA/B using AlphaFold 3(*28*). These models fail to predict high confidence interactions for the N or C terminus of CLMB. However, consistent with our NMR analyses, they do show two copies of phosphorylated CLMB simultaneously bound to CNA/B, one each at the LxVP and PxIxIT docking sites, with LxVP binding orienting phospho-Thr44 for dephosphorylation at the active site (Figure S2A-S2C). Thus, the formation of these multimeric complexes (2 CLMB: 1 CN) may facilitate dephosphorylation.

Calcineurin dephosphorylates CLMB by forming multimers. Our structural analyses suggest that CLMB can be dephosphorylated when in excess (2 CLMB: 1 CN), but not at lower CLMB:CN ratios, when phosphorylated CLMB is trapped in PxIxIT-bound complexes. To test this prediction, we inducibly expressed $CLMB_{WT}$ in HEK293 Flp-In T-REx cells alone or together with GFP-CNA. In stark contrast to its behavior with typical substrates, CNA overexpression led to increased CLMB phosphorylation (Figure 5A & S3A). Overexpressing catalytically inactive CN (GFP-CNA_{H151Q}), but not a mutant defective for PxIxIT binding (GFP-CNA_{NIR}), increased CLMB phosphorylation showing that intact PxIxIT binding rather than catalytic activity is required for this effect (Figure S3B). We then expressed GFP-CNA alone or alongside V5-tagged CLMB in HEK293 Flp-In T-REx cells inducibly expressing CLMB-FLAG to increase the CLMB:CN ratio. As predicted, the amount of phosphorylated $CLMB_{WT}$-FLAG observed in cells co-expressing GFP-CNA was reduced by introducing additional $CLMB_{WT}$-V5 (Figure 5A and B). This effect was dependent on PxIxIT binding as introducing $CLMB_{IxITMut}$-V5 did not decrease $CLMB_{WT}$-FLAG phosphorylation, but $CLMB_{LxVMut}$-V5, which contains an intact PxIxIT motif, did. We repeated these experiments using $CLMB_{IxITMut}$-FLAG, which is partially phosphorylated regardless of CN levels. Surprisingly, $CLMB_{IxITMut}$-FLAG was predominantly dephosphorylated when co-expressed with $CLMB_{WT}$-V5 or $CLMB_{LxVMut}$-V5 but not $CLMB_{IxITMut}$-V5 (Figure 5A and B). Thus, although the LxVP and PxIxIT

components of the CLMB composite motif are both required for efficient dephosphorylation, they do not need to be on the same molecule. A single copy of CLMB must have an LxVP to mediate its own dephosphorylation but can utilize the PxIxIT of neighboring copies to recruit CN, promote LxVP binding, and be dephosphorylated.

To determine quantitatively how the ratio of CLMB to CN affects dephosphorylation, we conducted a series of *in vitro* dephosphorylation assays using a fixed substrate concentration (100nM $pCLMB_{WT}$ or $pCLMB_{IxITMut}$ peptides) with varied CN concentrations (20nM, 100nM and 200nM). Increasing CN concentration accelerated the rate of dephosphorylation for $pCLMB_{IxITMut}$ while $pCLMB_{WT}$ showed no change (Figure 5C). We propose that this surprising result reflects the two different modes of CN-CLMB interaction: high affinity PxIxIT binding that prevents dephosphorylation and low affinity LxVP binding that is required for dephosphorylation. With a substrate that contains only an LxVP motif (i.e. $pCLMB_{IxITMut}$), increasing CN accelerates both LxVP association and dephosphorylation. However, with a substrate that contains a composite motif (i.e. $pCLMB_{WT}$), this increased LxVP binding is offset by an equivalent reduction in the amount of CLMB that is available for dephosphorylation due to PxIxIT-mediated CN-CLMB binding. We used kinetic modeling to assess how well this proposed mechanism explains the unique dynamics of CLMB dephosphorylation (Figure S2A and B). When simultaneously fitting $pCLMB_{WT}$ and $pCLMB_{IxITMut}$ dephosphorylation, the kinetic model was in good agreement with the data and estimated rate constants that approach expected values (Figure 5D and S2C)(*6, 22*). Together, these analyses provide evidence that the phosphorylated composite motif in CLMB confers unique attributes to its dephosphorylation. In addition to a requirement for Ca^{2+} and CaM, the presence of this composite motif dictates that substrate must be in excess of CN, allowing dephosphorylation to take place in multimeric complexes.

Discussion

In this study, we reveal how a composite LxVPxIxITxx(p)T motif functions in CN binding and dephosphorylation. For engaging CN, we can break down the thermodynamic contributions of the motif in CLMB into three parts: (i) the PxIxIT motif, (ii) phosphorylation of Thr44, and (iii) the LxVP motif. Peptide binding data reveal that the PxIxIT motif provides the largest contribution to the binding free energy, as we were unable to detect CLMB-CN binding using $CLMB_{IxITMut}$. Phosphorylation acts as the second major driver of binding affinity, imparting a ~30-fold increase in binding affinity, from K_D ~400nM to 13 nM for the non-phosphorylated versus phosphorylated peptide (Figure 3). Phosphorylation at this position also enhances the affinity of the PxIxIT motif in Cabin1, a CN regulator that like CLMB, contains a PxIxIT followed by "PP(p)TP"(*29, 30*). In contrast, mutation of the LxVP motif results only in a modest ~5-fold

reduction in binding affinity, indicating a smaller role in binding. These data suggest that the PxIxIT motif primarily anchors the peptide, while phosphorylation significantly enhances the overall affinity. We also measured the binding affinities with the CNA subunit, and the values, as well as the trends in binding affinities, remained consistent.

Using full length CLMB, NMR studies reveal that the binding interface for CN extends beyond the composite motif, with notable involvement of the N-terminal residues in interactions. However, this interaction may differ in a cellular environment, where the N-terminus is anchored to the membrane via S-acylation. At higher molar ratios of CLMB to CN, NMR data suggest that a second CLMB molecule can bind, likely utilizing the LxVP motif to engage the second binding site at the CNA /CNB heterodimeric interface. These findings are supported by *in vivo* data, showing that increasing CN expression enhanced levels of phosphorylated CLMB which then decreased when CLMB expression was further increased.

Based on all of our data, we present two models for how CLMB may shape CN activity *in vivo* (Figure 6). Dynamic S-acylation allows CLMB to associate with membranes (Figure 6A, Step 1), where, when phosphorylated, it recruits a localized pool of CN via high affinity PxIxIT-mediated binding (Figure 6A, Step 2). In the presence of a Ca^{2+} signal, Ca^{2+} and CaM activate CN which exposes the LxVP docking site(*31*). If CLMB is in excess relative to CN and PxIxIT binding is fully saturated, a second CLMB molecule will bind via its LxVP motif which positions phosphorylated Thr44 for dephosphorylation at the active site (Figure 6A, Step 3). As the population of CLMB shifts to this non-phosphorylated form, a decrease in PxIxIT binding affinity (Figure 3) promotes CN dissociation from CLMB, allowing CN to engage and dephosphorylate other nearby LxVP- and PxIxIT-containing substrates (Figure 6A, Step 4). A similar requirement for 'low' PxIxIT affinity was demonstrated for the AKAP5 scaffold, which binds and concentrates both CN and NFAT near L-type Ca^{2+} channels in neurons to promote NFAT dephosphorylation. However, increasing the affinity of the native PxIxIT in AKAP5 for CN ~two-fold significantly impaired NFAT activation due to sequestering of CN(*2*).

In our second model (Figure 6B), active CN-CLMB dimers (1 CLMB: 1 CN) directly engage and dephosphorylate substrates at the membrane that contain only an LxVP motif (Figure 6B, step 3). Many candidate CN substrates are predicted to contain only an LxVP, but if and how the majority are dephosphorylated by CN has yet to be uncovered. The best characterized example is the cAMP-dependent protein kinase type II-alpha regulatory subunit (PRKAR2A), which depends on the PxIxIT motif within its binding partner, AKAP5, to recruit CN for its dephosphorylation(*9, 32*). In our second model (Figure 6B), active CN-CLMB dimers (1 CLMB: 1 CN) directly engage and dephosphorylate such PxIxIT-less substrates at the membrane (Figure 6B, step 3). Simply recruiting CN to membranes, where association kinetics are 20-30 fold faster than in the cytosol of eukaryotic cells, may enhance LxVP binding such that

these substrates are efficiently dephosphorylated despite lacking their own PxIxIT motif(*33*). Division of the PxIxIT and LxVP motifs among two molecules may also allow for the extremely high affinity PxIxIT observed in CLMB. In substrates that contain both LxVP and PxIxIT motifs, stable PxIxIT binding may limit enzymatic efficiency by slowing product release. However, acting only as a scaffold, CLMB can remain tightly associated with CN via PxIxIT-binding while other substrates cycle in and out of the LxVP-binding surface and are dephosphorylated. In this scenario (Figure 6B), CN remains at the membrane either until CLMB levels increase sufficiently to allow CLMB dephosphorylation and CN dissociation (Figure 6B step 4) or until CLMB is deacylated. In both models, intracellular Ca^{2+} dynamics, CLMB protein levels, and S-acylation/de-acylation activities control CN signaling. Future studies aim to identify the palmitoyl acyltransferases (PATs) and acyl protein thioesterases (APTs) that dynamically regulate CLMB S-acylation to better understand how CN-CLMB signaling is controlled *in vivo*.

Another missing player in our model is the kinase(s) that phosphorylates CLMB. Because phosphorylation increases binding affinity, activation of the kinase is required to prime CLMB to regulate CN signaling. However, phosphorylation also establishes a negative feedback mechanism as dephosphorylation decreases CN's interaction with its own substrate. Thus, potential regulation of the kinase(s) that phosphorylates CLMB may significantly affect signaling dynamics. The stress-activated p38 mitogen-activated protein kinase (MAPK) phosphorylates the PP(p)TP site in Cabin1 and is predicted to phosphorylate Thr44 of CLMB(*34*). Therefore, future identification of the kinase(s) that phosphorylates CLMB may reveal additional mechanisms that regulate this signaling response.

Because this is the first composite motif to be analyzed, further studies are needed to establish whether dephosphorylation via multimeric complexes is a general property of such motifs. Several predicted LxVPxIxIT motifs occur in ion channels, such as TRPM6, that assemble into higher order complexes(*9, 35*). Thus, composite motifs, which are present in at least thirty additional human proteins, may in some cases provide a safety mechanism, to ensure that CN dephosphorylates only the multimeric forms of some substrates(*9*).

The major challenge that lies ahead is to identify the molecular targets and physiological functions that are regulated by CN-CLMB. When overexpressed in non-transformed fibroblasts, CN-CLMB increased invasion, and CLMB promotes proliferation and migration of some pancreatic ductal adenocarcinoma (PDAC) derived cell lines, suggesting that CLMB shapes CN signaling to regulate oncogenesis(*10*). Indeed, high CLMB expression is associated with poor patient outcomes for PDAC, melanoma and head and neck cancer(*10, 11*). Mechanisms underlying these activities have not yet been identified, but these cancers may provide good starting points for examining how CLMB modifies CN signaling in a biologically and clinically relevant context(*36*).

Materials and Methods

Cell culture and transfection:

Cells were cultured at 37 °C in 5% CO_2. HEK293 Flp-In TReX and MCF7 cell lines were grown in standard media containing Dulbecco's modified eagle's medium (DMEM) with 4.5 mg/mL glucose, L-glutamine, and sodium pyruvate (Cytiva SH30243.FS) supplemented with 10% fetal bovine serum (Corning MT35010CV). Transfections were done according to manufacturer instructions. HEK293 cells were transfected using lipofectamine 2000 (Thermo Fisher Scientific 11668019). MCF7 cells were transfected using Transfex ATCC transfection reagent (ATCC ACS-4005).

Stable cell line generation:

On day one, 9.6 x 10^5 HEK293 Flp-In TReX cells were transfected using lipofectamine 2000 with 1.5 µg pOG44 and 0. 5 µg pcDNA5 FRT TO encoding proteins of interest in a 6 well dish (plasmid # 2801, 2852, 2860, 2861, 2862, 2863, 2864, and 2880). Transfections were done according to manufacturer instructions. On day two, transfected cells were passaged onto 10cm plates. On day three, selection was started using media containing 3 µg blasticidin and 200 ng/mL hygromycin. Selection media was replaced every 2-3 days until distinct colonies appeared. Colonies were selected using cloning rings and expanded before being stored in liquid nitrogen.

Metabolic labeling to detect CLMB lipidation:

HEK293 Flp-In TReX lines stably expressing $CLMB_{WT}$, $CLMB_{C7,14S}$, or $CLMB_{G2A}$ were induced with 10 ng/mL doxycycline for 24 hours and split evenly among three 10 cm tissue culture dishes. The following day, cells were rinsed with PBS and incubated in DMEM containing 4.5 mg/mL glucose, L-glutamine, sodium pyruvate, 2% FBS, and either 20 µM YnMyr (Click Chemistry Tools 1164-5), 30 µM 17-ODYA (Cayman Chemical Company 34450-18-5), or vehicle (ethanol and DMSO) overnight. Cells were then co-incubated with 20 µM YnMyr, 30 µM 17-ODYA, or vehicle and 20 µM MG132 (EMD Millipore 474787-10MG) for 4 hours before washed twice in PBS and frozen at -80 °C. Cells were lysed in 400 µL TEA lysis buffer (50 mM TEA pH 7.4, 150 mM NaCl, 1% triton X-100, and 1 mM PMSF) by inverting for 15 minutes at 4 °C. Lysates were passed five times through a 27-gauge needle, centrifuged at 16,000 x *g* for 15 minutes at 4 °C and protein content determined by Pierce BCA protein assay kit (Thermo Fisher Scientific 23225). 25 µg total lysate was removed as input and 0.5 mg total protein was incubated with pre-washed magnetic M2 anti-FLAG (Sigma-Aldrich M8823-5ML) beads at 4 °C for 1.5 hours while inverting. Beads were washed 3X with modified RIPA (50 mM TEA pH 7.4, 150 mM NaCl, 1% Triton X-100, 0.1% SDS, and

1% sodium deoxycholate) and resuspended in 40 µL 1x PBS. 10 µL of 5x click reaction mix (1x PBS, 0.5 mM biotin azide, 5 mM TCEP, 0.5 mM TBTA, 5 mM $CuSO_4$) was added and reactions incubated for 1 hour at 24 °C, shaking at 550 RPM. Beads were washed 3X in modified RIPA and eluted 2X using 30 µL of 1 mg/mL FLAG peptide in modified RIPA buffer. 12 µL of non-reducing 6x SDS sample buffer was added to eluate before heating at 95 °C for 2 minutes and analysis by SDS-PAGE. Note that addition of reducing agents to SDS sample buffer results in loss of 17-ODYA signal. Samples were transferred to nitrocellulose membrane and lipidation was detected using fluorophore-tagged streptavidin, and total CLMB with anti-FLAG. Immunoblots were imaged using a Licor Odyssey CLx and quantified with Image Studio software.

Metabolic pulse-chase labeling assay to assess dynamic CLMB S-acylation:

HEK293 Flp-In TReX cells stably expressing $CLMB_{WT}$-FLAG were induced with 10 ng/mL doxycycline for 48 hours. Cells were rinsed 2X in PBS and incubated in methionine free DMEM supplemented with 5% charcoal-stripped FBS, 1 mM L-glutamate, 1 mM sodium pyruvate, 0.4 mM cysteine and 10 ng/mL doxycycline along with vehicle (ethanol), 30 µM 17-ODYA, 50 µM L-AHA, or 17-ODYA and L-AHA together. After two hours, cells were washed 2X in PBS and either harvested immediately or incubated in standard media supplemented with 10 µM palmitic acid and 10 ng/mL doxycycline, with or without 10 µM palmostatin B (EMD Millipore 178501-5MG). Cells were rinsed in PBS and frozen at -80 °C. Metabolic labeling was done as described in the previous section with the exception that two rounds of labeling were done. First, Cy5-azide (Click Chemistry Tools AZ118-1) was linked to 17-ODYA. Then, cells were washed and L-AHA was linked to AF-488 (Click Chemistry Tools 1277-1) alkyne before being washed three additional times and eluted using FLAG peptide. Samples were resolved via SDS-PAGE and in-gel fluorescence was read using the GE Amersham Typhoon imaging system. Images were quantified in Image Studio. The proportion of S-acylated CLMB is calculated as Cy5/A-488 normalized to the no chase control.

Acyl-PEG exchange:

HEK293 Flp-In TReX lines stably expressing $CLMB_{WT}$, $CLMB_{C7S}$, $CLMB_{C7,14S}$, or $CLMB_{G2A}$ were induced with 10 ng/mL doxycycline for 48 hours. Cells were rinsed 2X in PBS and stored at -80 °C. Cells were lysed in 400 µL lysis buffer (50 mM TEA pH 7.3, 150 mM NaCl, 2.5% SDS, 1 mM PMSF, 100 units benzonase) at 37 °C for 20 minutes, shaking at 800 RPM. Lysates were passed 10X through a 27-gauge needle, centrifuged at 16,000 x *g* for 5 minutes and protein quantified by BCA. Lysates were adjusted to 2 mg/mL and incubated with 10 mM TCEP for 30 minutes at room temperature. Cysteines were protected by incubating with 25 mM NEM for 2 hours at 40 °C, shaking at 800RPM. Protein was precipitated over night with four volumes of acetone at -20 °C, centrifuged at 16,000 x *g* for 20 minutes at 4 °C and washed 4X in 70% acetone. Acetone was removed, pellets air-dried to remove all traces of acetone and resuspended in 75

µL Buffer A (50 mM TEA pH 7.3, 150 mM NaCl, 4% SDS, 0.2% triton X-100, 4 mM EDTA) for 1 hour at 40 °C, shaking at 800 RPM. Samples were centrifuged at 16,000 x *g* for 2 minutes, 7 µL removed as input, and the remainder split into +cleavage and -cleavage fractions. The +cleavage sample containing 1% SDS was treated with 750 µM hydroxylamine (final concentration) for 1 hour at 30 °C, rotating end over end. Following methanol-chloroform precipitation (ice cold, final concentrations 42% methanol, 16% chloroform) samples were centrifuged at 16,000 x *g* for 20 minutes at 4 °C, aqueous layer removed, washed 3X with 100% methanol and air dried. Pellets were resuspended as described in Buffer A and incubated in 1 mM mPEG-Mal (Methoxypolyethylene glycol maleimide, 5 kDa, 63187 Sigma-Aldrich) for 2 hours at room temp, rotating end over end. Samples were methanol-chloroform precipitated as described, resuspended in Lysis buffer with 1X SDS-PAGE sample buffer, resolved using SDS-PAGE and visualized via immunoblotting with mouse anti-FLAG to detect CLMB-FLAG. Endogenous calnexin was detected using anti-calnexin antibodies. Immunoblots were imaged using a Licor Odyssey CLx and quantified with Image Studio software.

Detergent-assisted subcellular fractionation:

HEK293 Flp-In TReX lines stably expressing $CLMB_{WT}$, $CLMB_{C7,14S}$, or $CLMB_{G2A}$ were induced with 10 ng/mL doxycycline for 48 hours and 20 µM MG132 (EDM Millipore 474787-10MG) for 4 hours prior to harvesting. Cells were washed 2X in PBS, harvested and immediately lysed in 600 µL of Cytoplasm Buffer (10 mM HEPES pH 6.8, 100 mM NaCl, 300 mM sucrose, 3 mM $MgCl_2$, 5 mM EDTA, 0.015% digitonin, 1x halt protease inhibitor cocktail (Thermo Fischer scientific 78442)) at 4 °C for 15 minutes. 60 µL of total lysate was removed as input and the remainder centrifuged at 1000 x *g* for 10 min at 4 °C. The supernatant was removed as cytoplasmic fraction and the pellet washed 2X in PBS and resuspended in 600 µL membrane buffer (10 mM HEPES pH 7.5, 100 mM NaCl, 300 mM sucrose, 3 mM $MgCl_2$, 3 mM EDTA, 0.5% Triton X-100, 1x halt protease inhibitor cocktail) for 30 minutes at 4 °C turning end over end. Insoluble material was pelleted by centrifugation at 5000 x *g* for 10 minutes at 4 °C and supernatant removed as membrane fraction. Both fractions were centrifuged at 12,000 x *g* at 4 °C for 10 minutes. Samples were heated in 1X SDS sample buffer at 95 °C for 5 minutes, resolved via SDS-PAGE, immunoblotted and CLMB-FLAG detected using anti-FLAG antibodies; anti-GM130 and anti-α-tubulin were used as membrane and cytosolic markers respectively. Immunoblots were imaged using a Licor Odyssey CLx and quantified with Image Studio software. CLMB in cytosolic and membrane fractions were quantified as $CLMB_{Cyto}/(CLMB_{Cyto}+ CLMB_{Mem})$ and $CLMB_{Mem}/(CLMB_{Cyto} + CLMB_{Mem})$, respectively.

Immunofluorescence, microscopy, and image analysis:

MCF7 cells were co-transfected (as described previously) with equal amounts of pcDNA5 encoding $CLMB_{WT}$, $CLMB_{IxITMut}$, $CLMB_{LxVMut}$, $CLMB_{T44A}$ and pcDNA5 encoding CNA-GFP. The following day cells were plated on poly-lysine coated 12 mm, #1.5H glass coverslips (ThorLabs). On day three, cells were washed in PBS and fixed in 100% methanol for 10 minutes at -20 °C. Coverslips were washed 3 times in 1x PBS, blocked (1x PBS, 200 mM glycine, 2.5% FBS) for 30 minutes at room temperature, then incubated in primary antibody diluted in blocking buffer for 1 hour before being washed 3 times in 1x PBS and incubated for 1 hour in secondary antibody solution. Following three additional washes, coverslips were mounted using Prolong Glass mountant with NucBlue stain. After sitting overnight at room temperature, coverslips were imaged using a Lionheart FX automated widefield microscope with a 20X Plan Fluorite WD 6.6 NP 0.45 objective. For each coverslip, a 7 by 7 grid of non-overlapping images was automatically taken. All images were manually assessed and those with defects (debris, bubbles, out-of-focus, etc.) were filtered out. Images were analyzed using an automated pipeline using CellProfiler(*37*). Briefly, cells were identified by their nuclei and all those lacking CLMB-FLAG staining removed. CLMB-FLAG signal was used to define the cell body and all cells containing one or more fully saturated pixels in the CLMB-FLAG or CNA-GFP channels were removed. Pearson's correlation coefficient between CLMB-FLAG and CNA-GFP was determined for each individual cell. >500 cells per condition were analyzed.

GFP-Trap coimmunoprecipitation:

HEK293 cells were co-transfected (as described previously) with pcDNA5 encoding CNA-GFP and pcDNA5 encoding $CLMB_{WT}$, $CLMB_{IxITMut}$, $CLMB_{LxVMut}$, $CLMB_{T44A}$, or $CLMB_{LxVMut+T44A}$. 24 hours post-transfection, cells were washed 2X in PBS and frozen at -80 °C. Cells were lysed in 500 µL lysis buffer (50 mM Tris pH 7.5, 150 mM NaCl, 1% NP-40), aspirated 5X with a 27-gauge needle, centrifuged at 16,000 x *g* for 20 min at 4 °C and protein quantified via BCA. 100 mg total protein was removed as input. Lysates were adjusted to 0.5% NP-40 and 500 µg of protein incubated with pre-washed magnetic GFP-TRAP beads (ChromoTek gtma-20) for 2 hours at 4 °C, turning end over end. Beads were magnetized, washed 3 times and eluted with 50 µL of 2x SDS PAGE sample buffer. Samples were resolved via SDS-PAGE and visualized via immunoblotting with anti-flag antibodies to detect CLMB-FLAG and anti-GFP to detect CNA-GFP. Anti-GAPDH was used as a loading control for inputs. Immunoblots were imaged using a Licor Odyssey CLx and CLMB-calcineurin binding was quantified with Image Studio software. Co-purified CLMB was normalized using the following: $(CLMB_{IP}/CLMB_{Input})/GFP\text{-}CNA_{IP}$. Additionally, all values are displayed relative to $CLMB_{WT}$ which is set at 1.

Protein expression and purification:

CNA catalytic dead mutant H151Q with an N-terminal His_6-CNA (residues 1–391) and CNB (residues 1–170) subunits were expressed using *E. coli* BL21(DE3) cells in Lysogeny Broth (LB) supplemented with 50 µg/mL ampicillin. Protein expression was induced with 1 mM isopropyl β-d-1-thiogalactopyranoside (IPTG) at 18 °C. Cells were lysed using a Fisherbrand™ Model 505 Sonic Dismembrator and lysates were centrifuged at 46,000 × *g* at 4 °C for 45 minutes. The protein was purified by incubation with nickel-nitriloacetic acid (Ni-NTA) agarose resin (Qiagen) for 3h at 4 °C. The resin was washed with 50 mM Tris pH 8.0, 250 mM NaCl, 20 mM imidazole, and 1 mM TCEP. A buffer containing 50 mM Tris pH 8.0, 250 mM NaCl, 300 mM imidazole, and 1 mM TCEP was used for elution. CN was further purified by SEC (Superdex® 200 Increase 10/300 GL) using Phosphate-buffered saline (PBS) and $CaCl_2$ 1mM as the final buffer.

Flourescence polarization binding assay:

All FP measurements were performed on a multifunctional microplate reader (EnVision, Perkin Elmer) in black 384-well microplates (Corning, Cat No 3575) with 30 µL of the assay solution per well. 480-nm excitation and 535-nm emission filters were used for the FP measurements. In the FP saturation binding experiments, 5 nM FITC labeled peptides were mixed with increasing concentrations of calcineurin in PBS and 500 µM $CaCl_2$ buffer (from 0 to 25 µM). The FP values were plotted against the log of the protein concentrations, and the dissociation constant (apparent K_D) was obtained from the resulting sigmoidal curve as analyzed in GraphPad Prism 10.

Flourescence polarization competition assay:

For the competitive binding assay, a mixture containing 5 nM FITC-labeled CLMB peptides and CN (0.08 and 2 µM for CLMB vs PVIVIT experiments) was incubated with serial dilutions of unlabeled peptides for 30 minutes at room temperature. The FP values were determined, and the IC_{50} values, i.e., the concentrations required for 50% displacement of the FITC labeled peptide, were calculated in GraphPad Prism 10. The K_i values of competitive inhibitors were calculated based on a previously reported method(*38*), further adapted by(*39*). Briefly, the relation of K_i and IC_{50} in competitive inhibition as applied to protein-ligand–inhibitor (P–L–I) interactions, can be summarized by the following equation:

$$K_i = \frac{IC_{50}}{(\frac{\mathrm{L}}{K_d} + 1)}$$

Where L stands for the concentration of ligand, i.e., the FITC-labeled peptide used in the FP binding assay; and K_D corresponds to the dissociation constant of the same FITC-labeled peptide resulting from the performed FP binding assay.

ITC measurements:

Isothermal titration calorimetry (ITC) experiments were performed using an Affinity ITC from TA Instruments (New Castle, DE) equipped with an autosampler in a buffer containing 50 mM HEPES, pH 8.0, 150 mM NaCl, 1 mM TCEP, 500µM $CaCl_2$ at 25 °C. 40 µM protein solution in the calorimetric cell was titrated with 100 µM peptide solution using 0.5 µL injection in 200-sec intervals using stirring speed at 125rpm. The resulting isotherm was fitted with a single site model to yield thermodynamic parameters of ΔH, ΔS, stoichiometry, and K_D using NanoAnalyze software (TA instruments).

NMR analyses:

All NMR data were acquired using TopSpin3.4 (Bruker), processed with NMRPipe v.2020/2021 and analyzed with CCPNmr v3(*40, 41*). Structural biology applications were compiled by the SBGrid consortium. Three-dimensional (3D) NMR experiments were conducted on a Bruker spectrometer operating at 600 MHz, equipped with TCI cryoprobes and z-shielded gradients. Samples of approximately180-µM 2H-, ^{13}C- and ^{15}N-calcimembrin in 20 mM Hepes pH 6.9, 100 mM NaCl, 0.5 mM EDTA, 1 mM TCEP and 5% v/v ^{2}H2O were used. Temperature was set to 25˚C. Chemical shift assignments are deposited in the Biological Magnetic Resonance Bank (BMRB) under accession code 52641.

The NMR titration samples were prepared by adding unlabeled calcineurin A/B complex or unlabeled calcineurin subunit A into solutions of U-[^{15}N, D]-labeled calcimembrin (50 µM) to reach a ratio of 0.5:1 (25 µM unlabeled calcineurin) or 1:1 (50 µM unlabeled calcineurin). Two-dimensional (2D) spectra were acquired using SOFAST-HMQC on a Bruker 800 MHz Avance III spectrometer equipped with a TXO cryoprobe and z-shielded gradients(*42*). Data was processed using NmrPipe and analyzed with CCPNmr. Secondary structure prediction was analyzed using Talos-N(*26*).

AlphaFold 3 modeling:

CN-CLMB complex modeling was done using AlphaFold 3 on AlphaFold server(*28*). Modeling was done using truncated CNA_{1-491}, CNB, and two copies of CLMB phosphorylated at Thr44. Zn^{2+} and Fe^{3+} (found in the CN active site) and four Ca^{2+} ions (bound to CNB) were included in modeling. All images were generated in UCSF ChimeraX 1.8(*43*).

***In vivo* analysis of CLMB phosphorylation status:**

HEK293 FLIP-In TreX cells stably expressing $CLMB_{WT}$-FLAG, $CLMB_{IxITMut}$-FLAG, $CLMB_{LxVMut}$-FLAG, or $CLMB_{T44A}$-FLAG were transfected with empty vector or pcDNA5 FRT TO encoding CNA-GFP alongside empty vector or pcDNA5 FRT TO encoding $CLMB_{WT}$-V5, $CLMB_{IxITMut}$-V5, or $CLMB_{LxVMut}$-V5.

Protein expression was induced for 24 hours with 10 ng/mL doxycycline, cells washed 2X in PBS and stored at -80 °C. Cells were lysed (50 mM Tris pH 8, 150 mM NaCl, 1% NP-40, 0.1% SDS, 0.5% sodium dodecyl sulfate, 1x Halt protease inhibitor cocktail) and resolved via SDS-PAGE and detected via immunoblotting.

***In vitro* CLMB phospho-peptide dephosphorylation:**

$CLMB_{WT}$, $CLMB_{IxITMut}$, and $CLMB_{LxVMut}$ phospho-peptides were synthesized by Vivitide, resuspended in 10 mM Tris pH 8.0 and dephosphorylated at 26 °C in reaction buffer (50 mM Tris pH 8.0, 100 mM NaCl, 6 mM $MgCl_2$, 2 mM $CaCl_2$, 1 mM EGTA, 0.1 mg/mL BSA, 1 mM DTT, 0.5 µM MDCC-PBP (Thermo Scientific PV4406), 1 µM CaM (Millipore Sigma 208694-1MG)). Reactions were initiated by addition of CLMB peptide to a final concentration of 200nM. Reactions took place in a total of 50 µL in a corning black 96 well vessel and were monitored continuously via fluorescence emitted by phosphate bound MDCC-PBP (EX:425/ EM:460). Phosphate standards were used to convert fluorescence intensity to phosphate concentration. Data were analyzed using Prism software and the rate of phosphate production was obtained by fitting data to a single exponential.

Kinetic Modeling:

Dephosphorylation data were fit by simulation and non-linear regression using Kintek Explorer™. Sigma values for each individual replicate were obtained using the double exponential afit function. All replicates were simultaneously fit to the models described in supplemental figures 2A and 2B. Curve offsets capped at a maximum offset of 50nM. Substrate concentration was allowed to vary by 15% during fitting. Offsets and substrate concentrations for each curve and fit quality metrics are displayed in Tables S1-S3. Final graphs display averaged ($n \geq 5$) phosphate released at each timepoint with the corresponding fit.

Statistical analysis:

Statistical analysis was done using Graphpad Prism version 10.2.2. All data is displayed as representative images or mean values with standard deviation error bars unless otherwise noted. All data represent three independent experiments unless otherwise indicated in figure legends. Image analysis of CLMB-CN colocalization was conducted using the following number of cells: $CLMB_{WT}$ = 525, $CLMB_{IxITMut}$ = 641, $CLMB_{LxVMut}$ = 500, $CLMB_{T44A}$ = 517. Statistical significance was calculated using one-way analysis of variance (ANOVA) with corrections for multiple comparisons as indicated.

Data sharing plan:

All original scans of immunoblots, immunofluorescence images, and AlphaFold predictions can be accessed through Mendeley Data (to be made available upon publication). Plasmids and reagents will be shared upon request. NMR chemical shift assignments are deposited in the Biological Magnetic Resonance Bank (BMRB) under accession code 52641.

Acknowledgements:

We thank Norman Davey and members of the Cyert and Arthanari labs, in particular Angela Barth and Sneha Roy, for helpful discussion. We are grateful to Callie Wigington and Makena Pule for their early contributions to the project and to Rick Russell for feedback on the kinetic modeling. We thank Ilya Bezprozvanny for suggesting the name, calcimembrin.

Funding:

MSC and DAB are supported by NIH grant R35 GM136243. DAB also acknowledges support from NIH grant T32 GM007276. HA, JCR, SQ and TV acknowledge grant R01 GM136859 from NIH.

Author Contributions:

MSC, DAB, HA and JCR conceived the studies. SQ and TV provided early NMR analysis of CLMB-CN complexes. DAB, supervised by MSC, carried out experiments and analyzed data for Figures 1, 2, and 5, and prepared figures. JCR, supervised by HA, carried out experiments and analyzed data for Figures 3 and 4. TV carried out secondary structure analyses. DAB and MSC wrote the manuscript in consultation with HA and JCR.

References:

1. I. Ulengin-Talkish, M. S. Cyert, A cellular atlas of calcineurin signaling. *Biochim Biophys Acta Mol Cell Res* **1870**, 119366 (2023).
2. H. Li *et al.*, Balanced interactions of calcineurin with AKAP79 regulate Ca2+-calcineurin-NFAT signaling. *Nature structural & molecular biology* **19**, 337-345 (2012).
3. J. Aramburu, A. Rao, C. B. Klee, Calcineurin: from structure to function. *Curr Top Cell Regul* **36**, 237-295 (2000).
4. S. Grigoriu *et al.*, The molecular mechanism of substrate engagement and immunosuppressant inhibition of calcineurin. *PLoS biology* **11**, e1001492 (2013).
5. J. Roy, M. S. Cyert, Identifying New Substrates and Functions for an Old Enzyme: Calcineurin. *Cold Spring Harb Perspect Biol* **12**, (2020).
6. B. L. Brauer *et al.*, Leveraging New Definitions of the LxVP SLiM To Discover Novel Calcineurin Regulators and Substrates. *ACS Chem Biol* **14**, 2672-2682 (2019).
7. S. R. Sheftic, R. Page, W. Peti, Investigating the human Calcineurin Interaction Network using the piLxVP SLiM. *Scientific reports* **6**, 38920 (2016).
8. E. Tsekitsidou *et al.*, Calcineurin associates with centrosomes and regulates cilia length maintenance. *J Cell Sci* **136**, (2023).

9. C. P. Wigington *et al.*, Systematic Discovery of Short Linear Motifs Decodes Calcineurin Phosphatase Signaling. *Mol Cell* **79**, 342-358 e312 (2020).
10. T. Nakamura *et al.*, Overexpression of C16orf74 is involved in aggressive pancreatic cancers. *Oncotarget* **8**, 50460-50475 (2017).
11. M. Uhlen *et al.*, Towards a knowledge-based Human Protein Atlas. *Nat Biotechnol* **28**, 1248-1250 (2010).
12. M. F.S. *et al.*, Mechanisms and functions of protein S-acylation. *Nat Rev Mol Cell Biol*, (2024).
13. X. Chen *et al.*, Palmitoylation of A-kinase anchoring protein 79/150 modulates its nanoscale organization, trafficking, and mobility in postsynaptic spines. *Front Synaptic Neurosci* **14**, 1004154 (2022).
14. I. Ulengin-Talkish *et al.*, Palmitoylation targets the calcineurin phosphatase to the phosphatidylinositol 4-kinase complex at the plasma membrane. *Nat Commun* **12**, 6064 (2021).
15. J. F. Rual *et al.*, Towards a proteome-scale map of the human protein-protein interaction network. *Nature* **437**, 1173-1178 (2005).
16. T. Meinnel, C. Dian, C. Giglione, Myristoylation, an Ancient Protein Modification Mirroring Eukaryogenesis and Evolution. *Trends Biochem Sci* **45**, 619-632 (2020).
17. M. Blanc, F. P. A. David, F. G. van der Goot, SwissPalm 2: Protein S-Palmitoylation Database. *Methods Mol Biol* **2009**, 203-214 (2019).
18. T. Kushibiki *et al.*, Role of Dimerized C16orf74 in Aggressive Pancreatic Cancer: A Novel Therapeutic Target. *Mol Cancer Ther* **19**, 187-198 (2020).
19. M. C. Yap *et al.*, Rapid and selective detection of fatty acylated proteins using omega-alkynyl-fatty acids and click chemistry. *Journal of lipid research* **51**, 1566-1580 (2010).
20. A. Percher *et al.*, Mass-tag labeling reveals site-specific and endogenous levels of protein S-fatty acylation. *Proceedings of the National Academy of Sciences of the United States of America* **113**, 4302-4307 (2016).
21. F. J. Dekker *et al.*, Small-molecule inhibition of APT1 affects Ras localization and signaling. *Nat Chem Biol* **6**, 449-456 (2010).
22. D. K. Blumenthal, K. Takio, R. S. Hansen, E. G. Krebs, Dephosphorylation of cAMP-dependent protein kinase regulatory subunit (type II) by calmodulin-dependent protein phosphatase. Determinants of substrate specificity. *J Biol Chem* **261**, 8140-8145 (1986).
23. B. A. Perrino, L. Y. Ng, T. R. Soderling, Calcium regulation of calcineurin phosphatase activity by its B subunit and calmodulin. Role of the autoinhibitory domain. *J Biol Chem* **270**, 340-346 (1995).
24. J. Aramburu *et al.*, Affinity-driven peptide selection of an NFAT inhibitor more selective than cyclosporin A. *Science* **285**, 2129-2133 (1999).
25. H. Li, L. Zhang, A. Rao, S. C. Harrison, P. G. Hogan, Structure of calcineurin in complex with PVIVIT peptide: portrait of a low-affinity signalling interaction. *Journal of molecular biology* **369**, 1296-1306 (2007).
26. Y. Shen, A. Bax, Protein structural information derived from NMR chemical shift with the neural network program TALOS-N. *Methods Mol Biol* **1260**, 17-32 (2015).
27. R. Hendus-Altenburger *et al.*, Molecular basis for the binding and selective dephosphorylation of Na(+)/H(+) exchanger 1 by calcineurin. *Nat Commun* **10**, 3489 (2019).
28. J. Abramson *et al.*, Accurate structure prediction of biomolecular interactions with AlphaFold 3. *Nature* **630**, 493-500 (2024).
29. S. Lee *et al.*, The optimized core peptide derived from CABIN1 efficiently inhibits calcineurin-mediated T-cell activation. *Exp Mol Med* **54**, 613-625 (2022).
30. H. Q. Nguyen *et al.*, Quantitative mapping of protein-peptide affinity landscapes using spectrally encoded beads. *Elife* **8**, (2019).
31. S. J. Li *et al.*, Cooperative autoinhibition and multi-level activation mechanisms of calcineurin. *Cell research* **26**, 336-349 (2016).

32. T. W. Church *et al.*, AKAP79 enables calcineurin to directly suppress protein kinase A activity. *Elife* **10**, (2021).
33. W. Y. C. Huang, S. G. Boxer, J. E. Ferrell, Jr., Membrane localization accelerates association under conditions relevant to cellular signaling. *Proc Natl Acad Sci U S A* **121**, e2319491121 (2024).
34. J. L. Johnson *et al.*, An atlas of substrate specificities for the human serine/threonine kinome. *Nature* **613**, 759-766 (2023).
35. C. H. Huang, Y. C. Chen, C. C. Chen, Physical interaction between calcineurin and Cav3.2 T-type Ca2+ channel modulates their functions. *FEBS Lett* **587**, 1723-1730 (2013).
36. A. S. Manalan, C. B. Klee, Activation of calcineurin by limited proteolysis. *Proc Natl Acad Sci U S A* **80**, 4291-4295 (1983).
37. D. R. Stirling *et al.*, CellProfiler 4: improvements in speed, utility and usability. *BMC Bioinformatics* **22**, 433 (2021).
38. Y. Cheng, W. H. Prusoff, Relationship between the inhibition constant (K1) and the concentration of inhibitor which causes 50 per cent inhibition (I50) of an enzymatic reaction. *Biochem Pharmacol* **22**, 3099-3108 (1973).
39. R. Z. Cer, U. Mudunuri, R. Stephens, F. J. Lebeda, IC50-to-Ki: a web-based tool for converting IC50 to Ki values for inhibitors of enzyme activity and ligand binding. *Nucleic acids research* **37**, W441-445 (2009).
40. F. Delaglio *et al.*, NMRPipe: a multidimensional spectral processing system based on UNIX pipes. *J Biomol NMR* **6**, 277-293 (1995).
41. W. F. Vranken *et al.*, The CCPN data model for NMR spectroscopy: development of a software pipeline. *Proteins* **59**, 687-696 (2005).
42. P. Schanda, E. Kupce, B. Brutscher, SOFAST-HMQC experiments for recording two-dimensional heteronuclear correlation spectra of proteins within a few seconds. *J Biomol NMR* **33**, 199-211 (2005).
43. E. C. Meng *et al.*, UCSF ChimeraX: Tools for structure building and analysis. *Protein Sci* **32**, e4792 (2023).

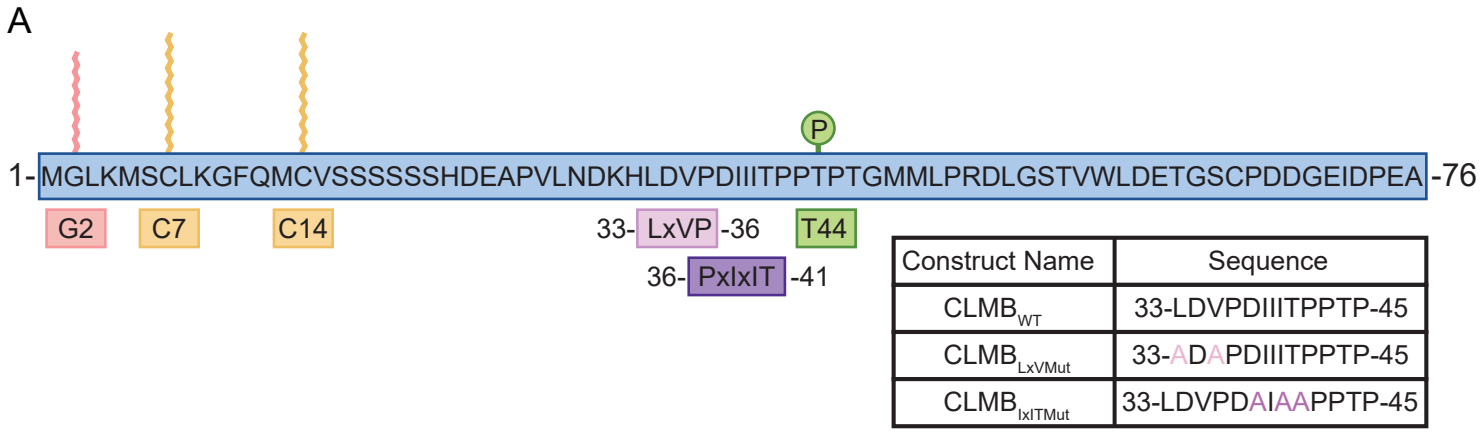

Construct Name	Sequence
$CLMB_{WT}$	33-LDVPDIIITPPTP-45
$CLMB_{LxVMut}$	33-ADAPDIIITPPTP-45
$CLMB_{IxITMut}$	33-LDVPDAIAAPPTP-45

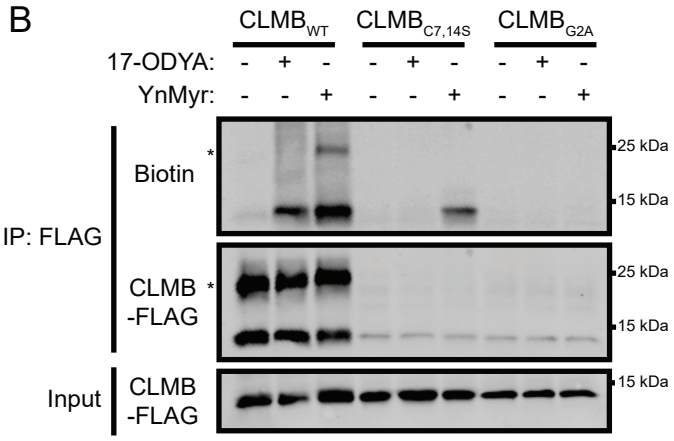

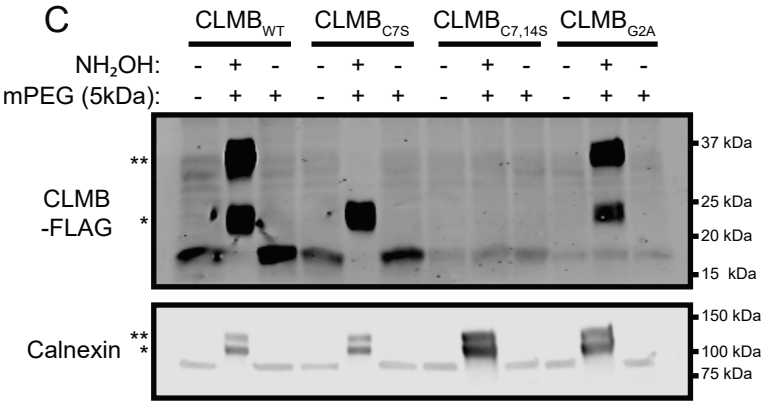

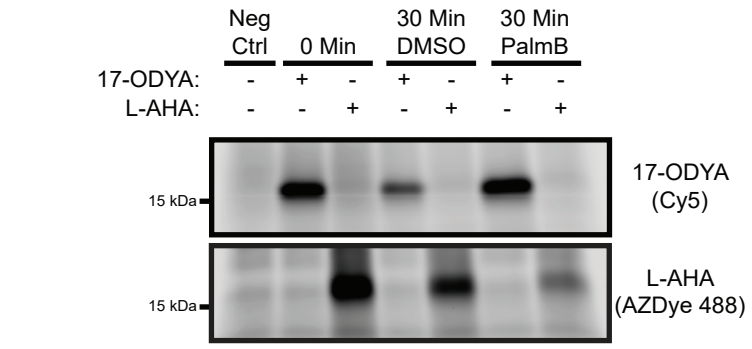

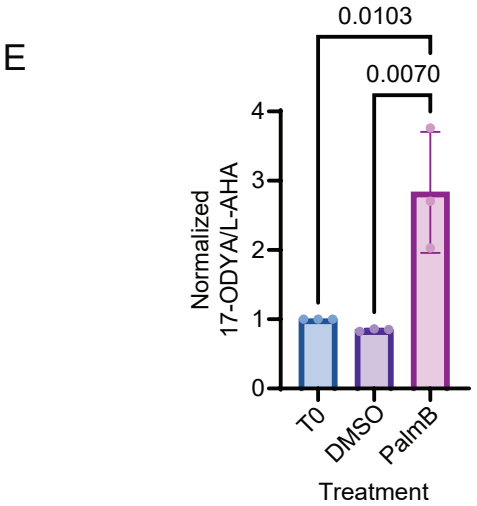

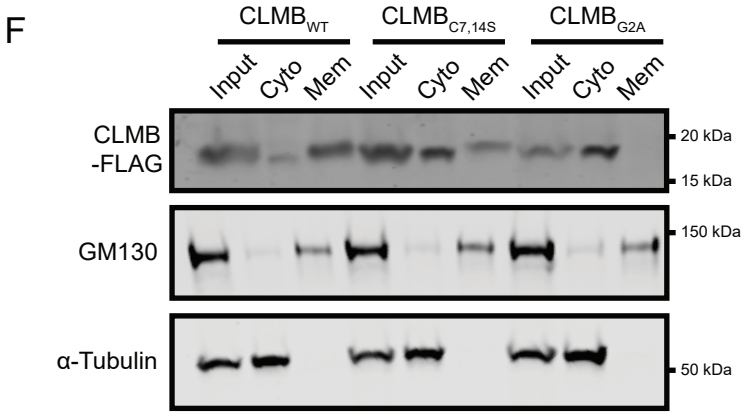

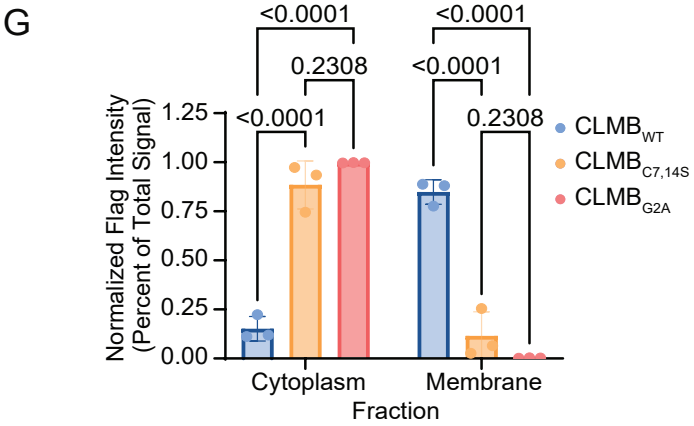

Figures Legends:

Figure 1: Calcimembrin localizes to membranes via protein lipidation.

a Schematic of CLMB. N-myristoylation (red); S-acylated cysteines (yellow); phospho-Thr44 (green); CN binding motifs LxVP (pink) and PxIxIT (purple). Mutant sequences are shown for $CLMB_{LxVMut}$ and $CLMB_{IxITMut}$.

b CLMB incorporates analogs of palmitate (17-ODYA) or myristate (YnMyr) as indicated. Cells were treated with 20 µM MG132 prior to harvesting. Representative immunoblot shown of FLAG tagged CLMB wild type ($CLMB_{WT}$), S-acylation defective ($CLMB_{C7,14S}$) or myristoylation defective ($CLMB_{G2A}$), immunoprecipitated and detected using CLICK chemistry with biotin-azide followed by detection with IRdye 800CW streptavidin (n = 3 independent experiments). Asterisks indicate CLMB dimers formed due to absence of reducing agents (see methods).

c Representative immunoblot of acyl-PEG exchange performed on lysates expressing $CLMB_{WT}$-FLAG or lipidation mutants ($CLMB_{C7S}$, $CLMB_{C7,14S}$, $CLMB_{G2A}$). PEGylation events, a proxy for S-acylation, are indicated by asterisks. For each sample, input, cleaved (NH_2OH) and PEGylated (mPEG), and non-cleaved PEGylated conditions are shown. Cells were treated with 20 µM MG132 for 4 hours prior to harvesting. Endogenous, dually S-acylated calnexin is a positive control (n = 3 independent experiments).

d Pulse chase analysis of CLMB-FLAG S-acylation turnover using analogs of palmitate (17-ODYA) or methionine (L-AHA). Incorporation into immunoprecipitated CLMB-FLAG in the absence of analog (Neg Ctrl), or after 2 hours of analog treatment followed by 0 or 30 minutes without analog including DMSO (control) or palmostatin B. 17-ODYA or L-AHA were detected using CLICK with Cy5 and AZDye 488, respectively. A representative in-gel fluorescence scan is shown (n = 3 independent experiments).

e Data from (**d**) showing mean ± SEM of 17-ODYA signal normalized to L-AHA. Indicated p-values calculated by two-way ANOVA corrected by Tukey's multiple comparison test. N=3 independent experiments.

f Sub-cellular fractionation of lysates containing $CLMB_{WT}$-FLAG or lipidation mutants ($CLMB_{C7,14S}$, $CLMB_{G2A}$). Cells were treated with 20 µM MG132 for 4 hours prior to harvesting. Representative immunoblot showing input, cytoplasmic (cyto), and membrane (mem) fractions. GM130 and α-tubulin mark membrane and cytosolic fractions respectively.

g Data from (**f**) showing mean ± SEM cytoplasmic or membrane signals normalized to total (cytoplasmic + membrane signals). Indicated p-values calculated by two-way ANOVA corrected by Tukey's multiple comparison test. N= 3 independent experiments.

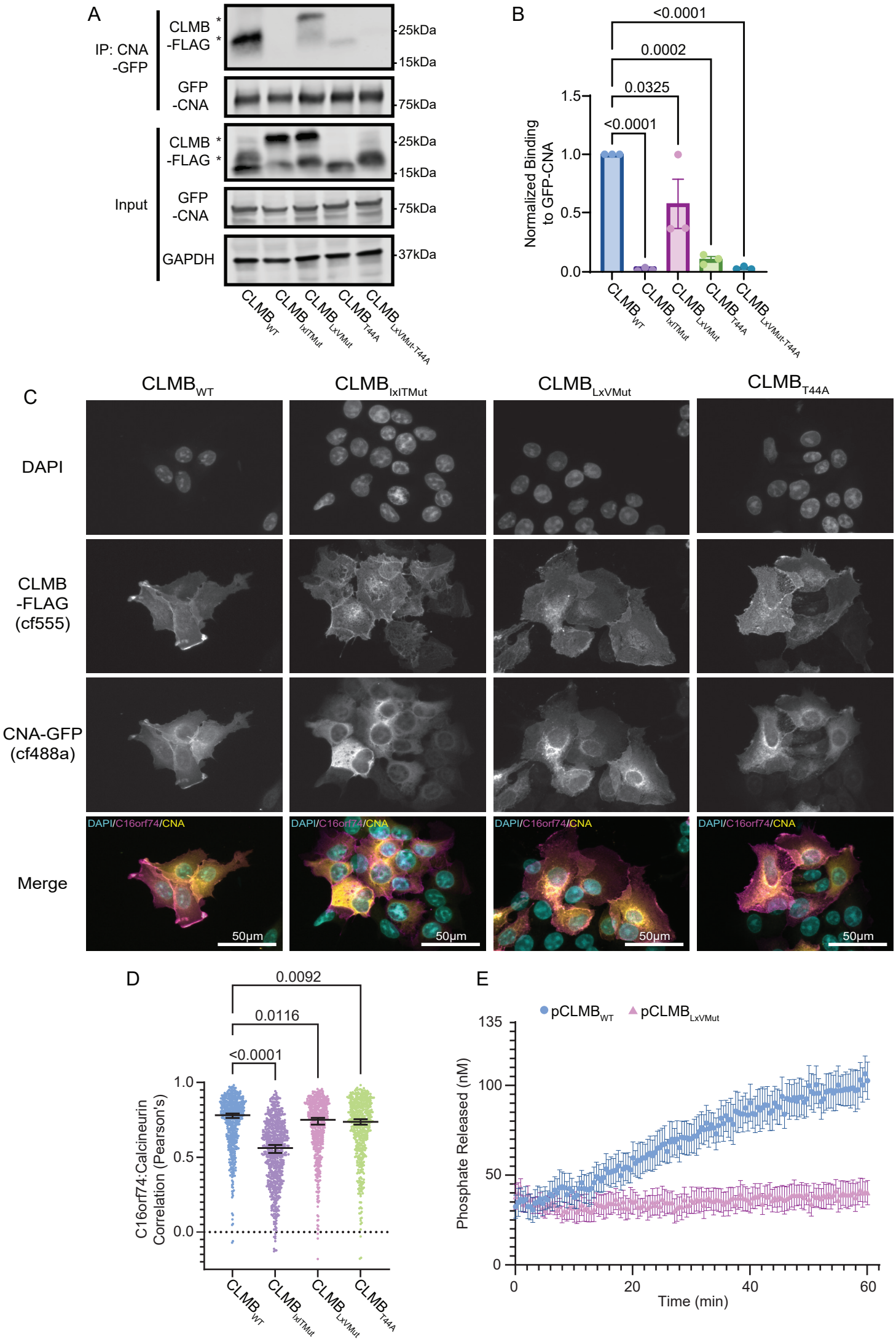
A
IP: CNA -GFP
CLMB -FLAG
GFP -CNA
Input
CLMB -FLAG
GFP -CNA
GAPDH
25kDa
15kDa
75kDa
37kDa
CLMB WT
CLMB IxITMut
CLMB LxVMut
CLMB T44A
CLMB LxVMut-T44A
B
Normalized Binding to GFP-CNA
<0.0001
0.0002
0.0325
<0.0001
C
CLMB WT
CLMB IxITMut
CLMB LxVMut
CLMB T44A
DAPI
CLMB -FLAG (cf555)
CNA-GFP (cf488a)
Merge
DAPI/C16orf74/CNA
50µm
D
C16orf74:Calcineurin Correlation (Pearson's)
0.0092
0.0116
<0.0001
E
pCLMB WT
pCLMB LxVMut
Phosphate Released (nM)
Time (min)

Figure 2: Composite SLiM in calcimembrin mediates binding to and dephosphorylation by calcineurin.

a Representative immunoblot of anti-GFP purification from lysates of HEK293 cells co-transfected with CNA-GFP and CLMB-FLAG ($CLMB_{WT}$, $CLMB_{IxITMut}$, $CLMB_{LxVMut}$, $CLMB_{T44A}$, or $CLMB_{LxVMut+T44A}$).

b Data from (**a**) showing mean ± SEM CLMB-FLAG pulled down normalized to CLMB-FLAG input levels and CNA-GFP pulled down. Indicated p-values calculated by two-way ANOVA corrected by Dunnett's multiple comparison test (n = 3 independent experiments).

c Representative immunofluorescence images of fixed MCF7 cells co-transfected with CLMB-FLAG ($CLMB_{WT}$, $CLMB_{IxITMut}$, $CLMB_{LxVMut}$, or $CLMB_{T44A}$) and CNA-GFP. CLMB was visualized using anti-FLAG, CN with anti-GFP, and nuclei with Hoechst 33342. Scale bar = 50 µm.

d Data from (**c**) showing median with 95% CI Pearson's correlation coefficient of CLMB-CN colocalization. Each point represents a single cell ($n \geq 500$ for each condition). Indicated p-values calculated by Kruskal-Wallis with Dunn's multiple comparisons correction.

e Plot of phosphate released from 200 nM $pCLMB_{WT}$ (blue circles) or $pCLMB_{LxVMut}$ (pink squares) phospho-peptides dephosphorylated by 20 nM CN and 1 µM CaM. Displayed is the mean ± SEM of phosphate released for ≥ 4 replicates at each timepoint.

A

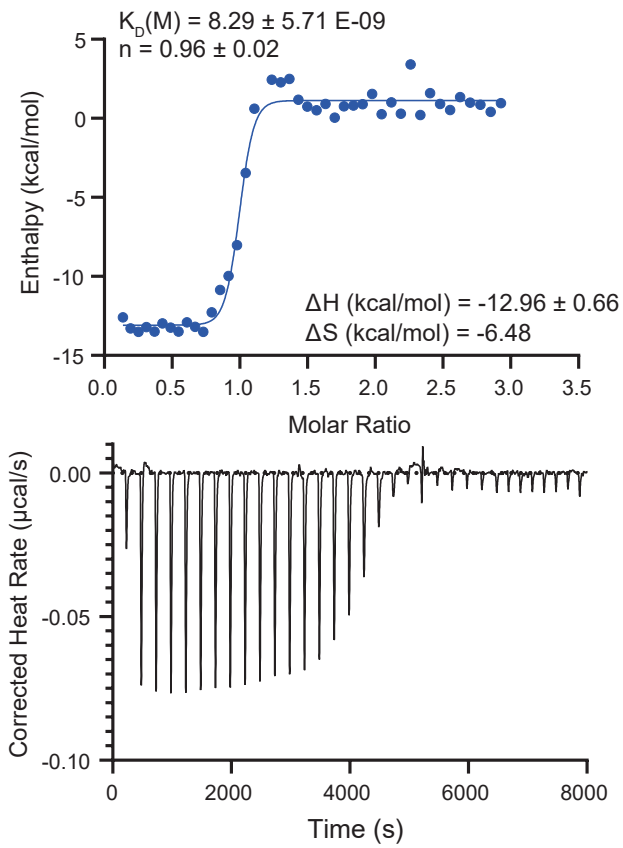

B

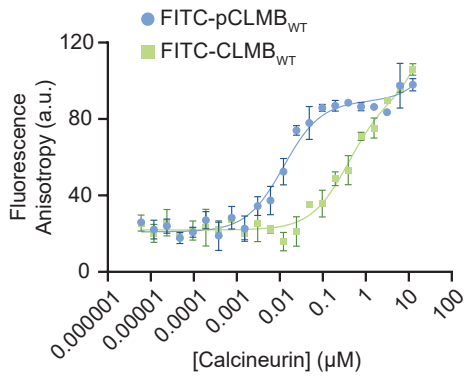

C

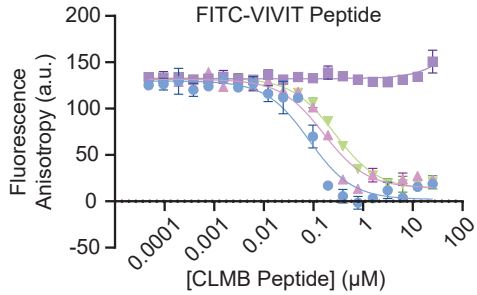

D

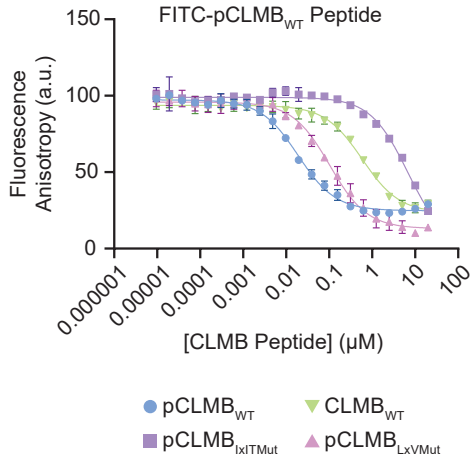

E

Peptide Competitor	FITC-VIVIT		FITC-pCLMB$_{WT}$	
	IC_{50}(nM)	K_i(nM)	IC_{50}(nM)	K_i(nM)
pCLMB$_{WT}$	81.4 ± 16.2	80.9 ± 16.1	18.9 ± 1.2	13.4 ± 0.8
pCLMB$_{IxITMut}$	NA	NA	6687 ± 878	4754 ± 624
pCLMB$_{LxVMut}$	159 ± 30	158± 30	103 ± 9	73.2 ± 6.4
CLMB$_{WT}$	267 ± 21	265 ± 21	585 ± 57	426 ± 40

Figure 3: Phosphorylation and the LxVP motif contribute to PxIxIT binding.

a Isothermal calorimetric enthalpy change displaying the thermometric evaluation of the affinity between CNA/B complex and unlabeled pWT peptide (top), and binding isotherm obtained by titration of unlabeled pWT into CNA/B complex (40 μM) (bottom). A dissociation constant (K_D) = 8.3 ± 5.7 nM was obtained.

b Fluorescence polarization (FP) saturation binding curves of two different FITC-labeled peptide tracers (5nM), FITC-pCLMB$_{WT}$ and FITC-CLMB$_{WT}$ were incubated with serial dilutions of CN A/B complex (0 to 12.5μM). The FP values were recorded at room temperature after a 30 minute incubation time. FP data were fitted to a one-site binding model (mean ± s.d., n = 2 independent experiments) using GraphPad Prism 10.0.

c Competitive binding assay of unlabeled pCLMB$_{WT}$, CLMB$_{WT}$, pCLMB$_{IxITMut}$, and pCLMB$_{LxVMut}$ peptides. The unlabeled peptides were titrated against a constant concentration of FP probe (FITC-PVIVIT peptide, 5 nM) in the presence of 2 μM CNA/B complex. Data (mean ± s.d., n = 2 independent experiments) were analyzed in GraphPad Prism 10.0.

d Competitive binding assay of unlabeled pCLMB$_{WT}$, CLMB$_{WT}$, pCLMB$_{IxITMut}$, and pCLMB$_{LxVMut}$ peptides. The unlabeled peptides were titrated against a constant concentration of FP probe (FITC-pCLMB$_{WT}$ peptide, 5 nM) in the presence of 0.08 μM CNA/B complex. Data (mean ± s.d., n = 2 independent experiments) were analyzed in GraphPad Prism 10.0.

e Table displaying the experimentally obtained IC_{50} values and converted K_i values resulting from the competitive binding assay of unlabeled pCLMB$_{WT}$, CLMB$_{WT}$, pCLMB$_{IxITMut}$, and pCLMB$_{LxVMut}$ peptides. The unlabeled peptides were titrated against a constant concentration of FP probe (FITC-pCLMB$_{WT}$ or FITC-PVIVIT, 5 nM) in the presence of 0.08 μM and 2μM CNA/B complex, respectively. Data (mean ± s.d., n = 2 independent experiments) were analyzed in GraphPad Prism 10.0.

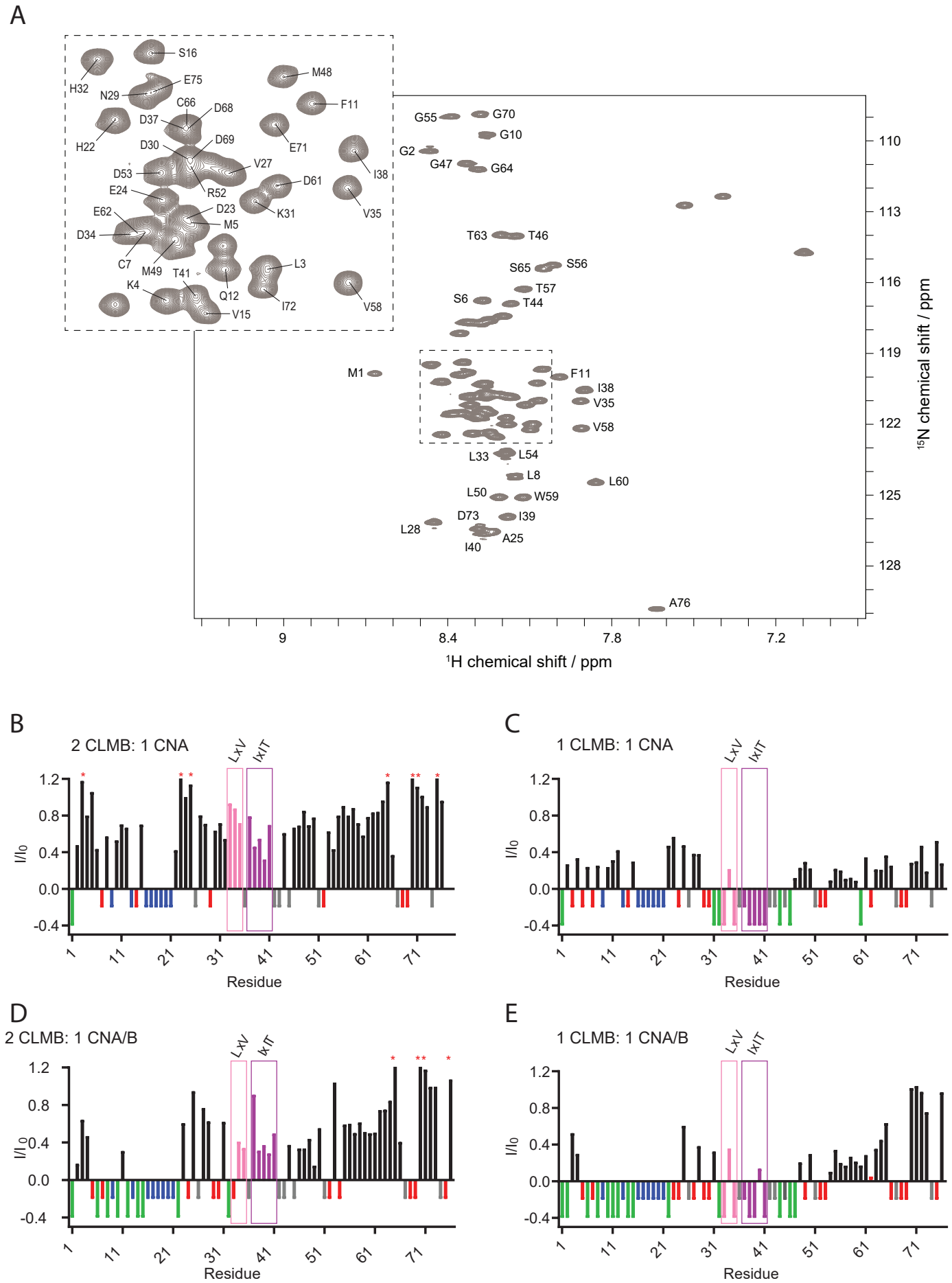
A
S16
H32
E75
N29
M48
F11
C66
D68
D37
H22
D30
D69
E71
D53
V27
I38
E24
R52
D61
E62
D23
K31
V35
D34
M5
C7
M49
T41
L3
K4
Q12
I72
V58
V15
G55
G70
G10
G2
G47
G64
T63
T46
S65
S56
T57
S6
T44
M1
F11
I38
V35
V58
L33
L54
L8
L60
L50
W59
D73
I39
L28
A25
I40
A76
110
113
116
119
122
125
128
9
8.4
7.8
7.2
^{1}H chemical shift / ppm
^{15}N chemical shift / ppm
B
2 CLMB: 1 CNA
LxV
IxIT
I/I0
Residue
C
1 CLMB: 1 CNA
LxV
IxIT
I/I0
Residue
D
2 CLMB: 1 CNA/B
LxV
IxIT
I/I0
Residue
E
1 CLMB: 1 CNA/B
LxV
IxIT
I/I0
Residue

Figure 4: **CLMB-CN binding extends beyond the LxVP and PxIxIT motifs.**

a ^{15}N HSQC spectra of free CLMB with the resonance assignment (red).

b NMR spectral analysis of the interaction of CLMB with CNA at 2:1 (CLMB: CNA); **c** with CNA at 1:1 (CLMB: CNA); **d** with CNA/B complex at 2:1 (CLMB: CNA/B); **e** with CNA/B complex at 1:1 (CLMB: CNA/B). The graphs display the intensity ratios of the CLMB resonances with and without the titrant (CNA or CNA/B) at different molar ratios. The ratios corresponding to the LxV motif, represented in pink, and IxIT motif, in purple. Residues where we cannot access the intensity ratio are represented with negative numbers. Peaks resulting in complete broadening are shown as negative bars in green (I/I_0 = -0.4). Residues that were not assigned in the apo CLMB are shown in blue (I/I_0 = -0.2), prolines that are not represented in a ^{15}N-HSQC are shown in grey (I/I_0 = -0.2), and residues where we cannot unambiguously assign the bound resonance is shown in red, (I/I_0 = -0.2). Residues that have an overlap in the resonance and hence when one of the resonances broadens results in I/I_0 higher than 1 is marked with a * sign.

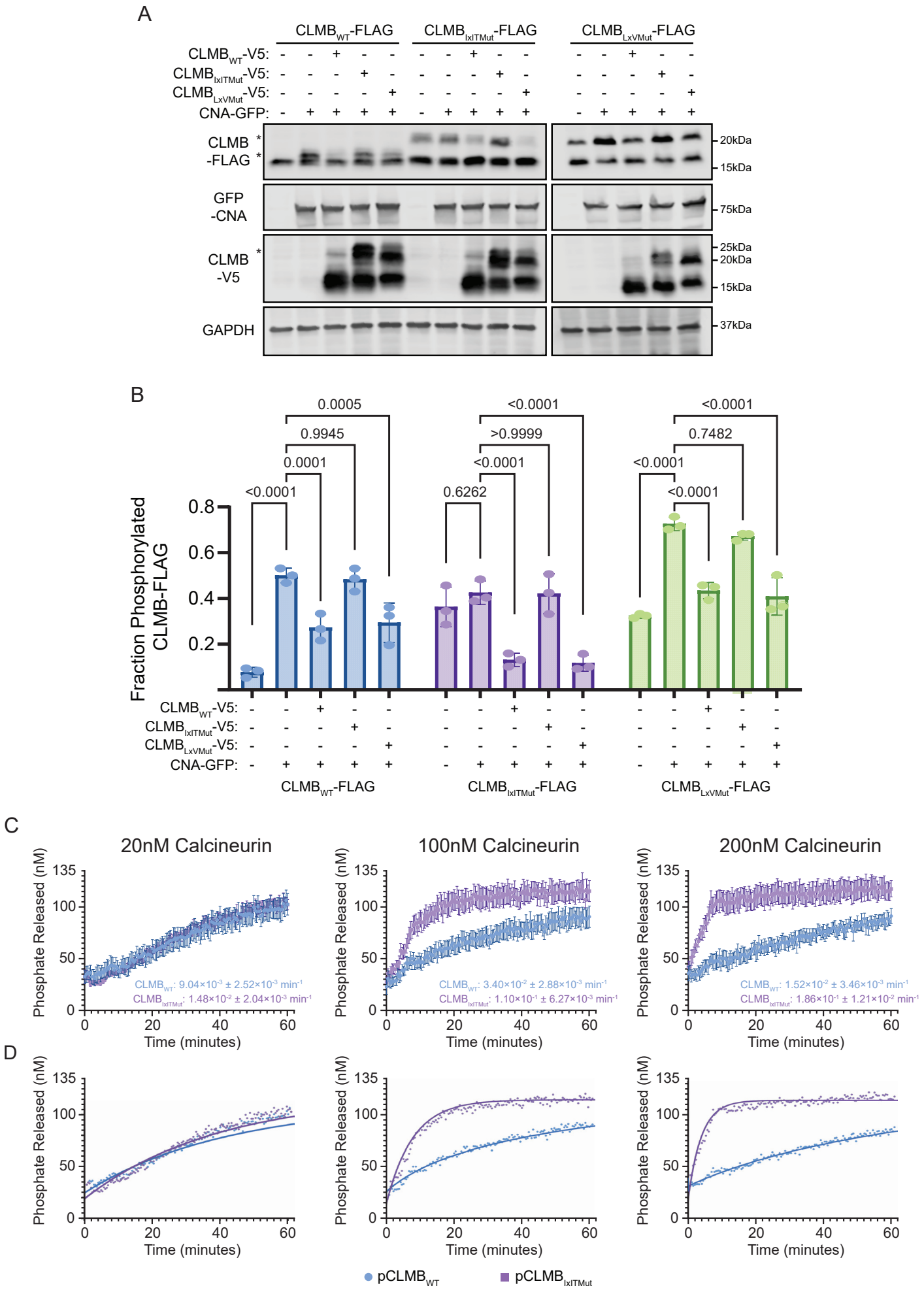
A
CLMB$_{WT}$-FLAG
CLMB$_{IxITMut}$-FLAG
CLMB$_{LxVMut}$-FLAG
CLMB$_{WT}$-V5:
CLMB$_{IxITMut}$-V5:
CLMB$_{LxVMut}$-V5:
CNA-GFP:
CLMB -FLAG
GFP -CNA
CLMB -V5
GAPDH
20kDa
15kDa
75kDa
25kDa
20kDa
15kDa
37kDa
B
Fraction Phosphorylated CLMB-FLAG
0.8
0.6
0.4
0.2
0.0005
0.9945
0.0001
<0.0001
<0.0001
>0.9999
<0.0001
0.6262
<0.0001
0.7482
<0.0001
<0.0001
CLMB$_{WT}$-V5:
CLMB$_{IxITMut}$-V5:
CLMB$_{LxVMut}$-V5:
CNA-GFP:
CLMB$_{WT}$-FLAG
CLMB$_{IxITMut}$-FLAG
CLMB$_{LxVMut}$-FLAG
C
20nM Calcineurin
100nM Calcineurin
200nM Calcineurin
Phosphate Released (nM)
Time (minutes)
CLMB$_{WT}$: 9.04×10^{-3} ± 2.52×10^{-3} min^{-1}
CLMB$_{IxITMut}$: 1.48×10^{-2} ± 2.04×10^{-3} min^{-1}
CLMB$_{WT}$: 3.40×10^{-2} ± 2.88×10^{-3} min^{-1}
CLMB$_{IxITMut}$: 1.10×10^{-1} ± 6.27×10^{-3} min^{-1}
CLMB$_{WT}$: 1.52×10^{-2} ± 3.46×10^{-3} min^{-1}
CLMB$_{IxITMut}$: 1.86×10^{-1} ± 1.21×10^{-2} min^{-1}
D
pCLMB$_{WT}$
pCLMB$_{IxITMut}$

Figure 5: Calcineurin dephosphorylates calcimembrin by forming multimers.

a Representative immunoblot of CLMB-FLAG phosphorylation-induced mobility shifts induced by CN overexpression. Performed using lysates from Flp-In-T-REx HEK cells inducibly expressing $CLMB_{WT}$-FLAG, $CLMB_{IxITMut}$-FLAG, or $CLMB_{LxVMut}$-FLAG and transfected with empty vector, CNA-GFP, or CNA-GFP with CLMB-V5 ($CLMB_{WT}$, $CLMB_{IxITMut}$, $CLMB_{LxVMut}$). Asterisks indicate phosphorylated CLMB.

b Data from (**a**) showing mean ± SEM phospho-CLMB-FLAG normalized to total CLMB-FLAG. Displayed p-values calculated by two-way ANOVA corrected by Dunnett's multiple comparison test (n = 3 independent experiments).

c Plots of phosphate released from 100 nM $pCLMB_{WT}$ (blue circles) or $pCLMB_{IxITMut}$ (purple squares) phosphopeptide dephosphorylated by 20 nM (left), 100 nM (middle) or 200 nM (right) CN and 1 μM calmodulin. Displayed is the mean ± SEM of phosphate released for ≥ 5 replicates at each timepoint.

d Plots as described in **c** fit by simulation to the model shown in S2A and S2B using Kintek Explorer.

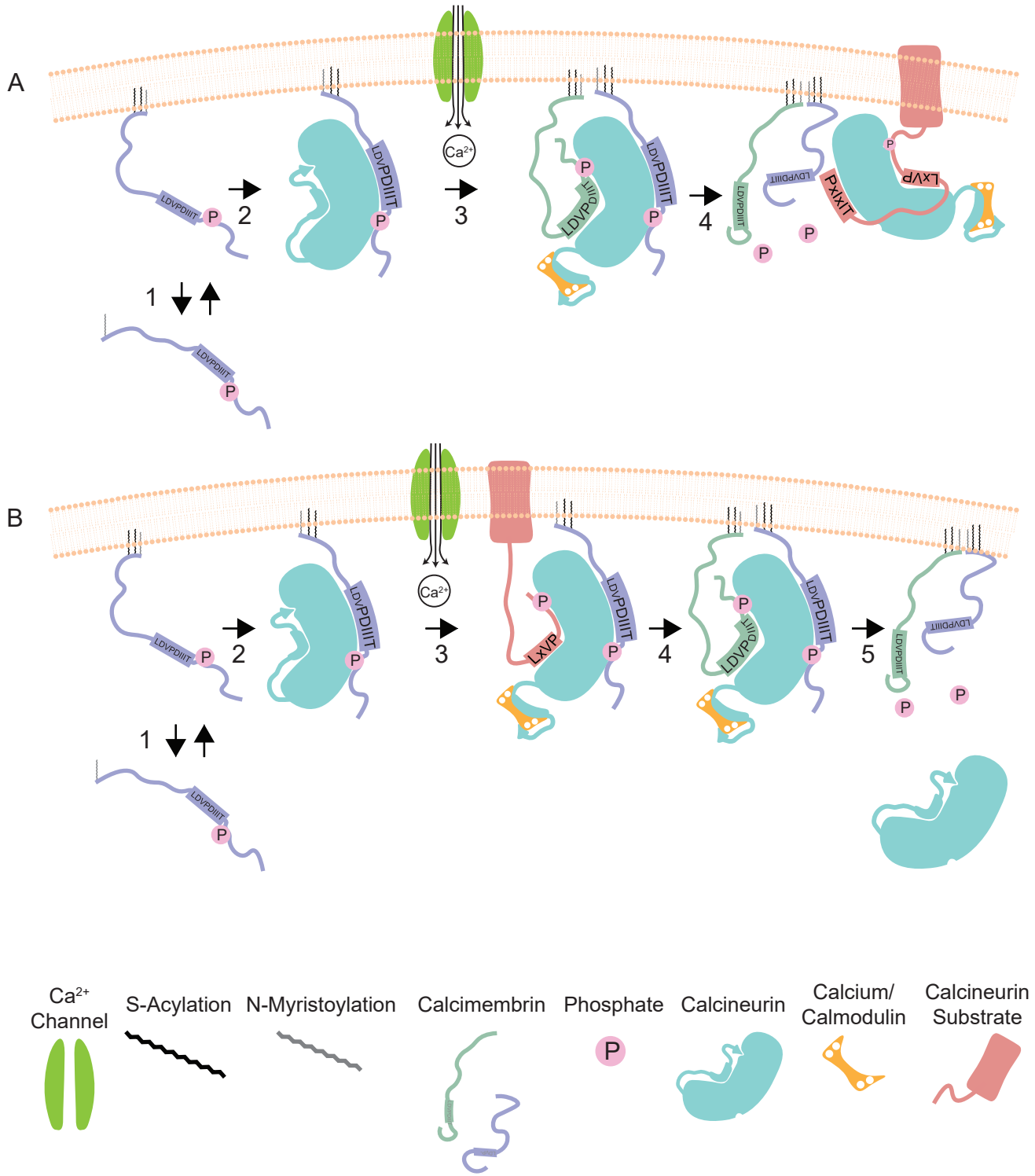
A
B
1
2
3
4
5
Ca2+
LDVPDIIIT
P
LXVP
PxIxIT
Ca2+ Channel
S-Acylation
N-Myristoylation
Calcimembrin
Phosphate
Calcineurin
Calcium/ Calmodulin
Calcineurin Substrate

Figure 6: A model for how calcimembrin modulates calcineurin signaling.

a (1) CLMB is dynamically acylated and localizes to membranes where it (2) recruits CN. When CLMB levels are low, CN remains tightly bound to phosphorylated CLMB regardless of Ca^{2+} signals. (3) As CLMB levels rise, Ca^{2+} and CaM binding allow CN-CLMB multimers to form and CLMB to be dephosphorylated. (4) CN is then freed to engage and dephosphorylate nearby substrates, activating CN signaling.

b (1) CLMB is dynamically acylated and localizes to membranes where it (2) recruits CN. When CLMB levels are low, CN remains tightly bound to phosphorylated CLMB. (3) Ca^{2+} and CaM activate CN, allowing CLMB to present it to nearby substrates for LxVP-mediated binding and dephosphorylation. (4) When CLMB accumulates at membranes, CN-CLMB multimers form, and (5) dephosphorylation triggers CN release, terminating CN signaling.